Contact Localization via Active Oscillatory Actuation

Divas Subedi, Elizabeth Schoemer, Digesh Chitrakar, Yun-Hsuan Su and Kevin Huang

***Abstract*— Many robotic tasks rely on physical interactions with the task environment. Sensing when and where links make physical contacts can be crucial in several applications, including but not limited to grasping, locomotion, collaborative robotics and navigation. While sensorizing robot end effectors with intrinsic tactile devices is a logical approach, current and accessible options are often expensive or require invasive modifications. This paper presents a prototype method of both sensing and localizing contacts along a rigid link that can be readily incorporated into existing machines. The mechanism is lightweight and low-cost, and functions by actively providing an oscillatory mechanical actuation signal to a rigid link, whose mechanical response is measured with an inertial device and is used to localize touch at one of five designated contact points. Classification is performed with supervised methods using transient behavior and spectral features. Evaluation is conducted with five-fold cross validation, and preliminary results indicate promising performance in localizing the point of contact on the rigid link with accuracy of over 97%.**

***Index Terms*— contact localization; active sensing; sensors; Mel-frequency cepstrum; machine learning;**

I. Introduction

A. Background

Robots capable of dexterous manipulation and other physical interactions like grasping can be deployed in unstructured environments like hospitals [1], [2], service industries, search and rescue [3], restaurants, and even space [4] with positive outcomes. Oftentimes interaction objects may be of high-value or delicate in nature, e.g. in robotic surgery [5]–[7] or human-robot interaction [8]. In such scenarios, it is of utmost importance that the robot minimizes risk of physical damage to delicate structures or assets. To do so, a robot should be aware of the physical contacts it makes with the environment, handle fragile objects, as well as be able to navigate through unknown or occluded spaces.

To model a 3D task space, a robot typically utilises several perceptual modalities such as vision, touch, or sound. While cameras and lidars are often used to gather ranging information from large areas, tactile sensors can be instrumental in reducing uncertainty and gaining additional information at a finer scale from the physical interaction between objects and an end effector [9]. Tactile robotic sensors attempt to replicate human touch capabilities, including haptic perception of textures and shape, via the detection of minute contact forces between a sensor and an external surface [10]. The tactile sensing technologies, whether using coupled or non-coupled electrical and mechanical transduction methodologies, struggle with high costs and high density actuator configurations depleting space efficiency [11]–[13]. The robotic ability to detect minor contact events at various locations along a serial linkage structure is often conducted through expensive pressure or temperature triggered systems [14] creating the desire for a low-cost and non-intrusive alternative sensor.

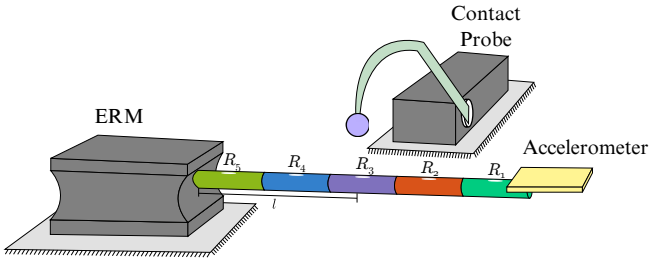

Fig. 1. Contact localization hardware setup.

Contact localization, in some vision [15] and tactile [16] based approaches, has sought to increase accuracy for grasping mechanisms between robotic end effectors and compact structures. With extended applications in human-machine assembly processes and locomotion, perception and localization of contact occurrences is needed. This work introduces an approach that is readily incorporated into rigid links, and is operated by actively vibrating and measuring the mechanical response to distinguish six different contact states, as shown in Fig. 1. The workflow is shown in Fig. 2.

B. Related Works

1) Contact Localization: Molchanov et al. [16] estimated environmental impacts along a robotic surface through a biomimetic tactile sensor (BioTac) with a data analysis driven approach of regression and classification methodology of clustered pressure frequencies in the time domain. Similarly, McMahan et al. [17] distributed multiple accelerometers along a Willow Garage PR2 for accurate contact event location via vibration detection. Prior research utilizing an excited single link elastic contact model demonstrated the sensitivity of contact force detection across said system as compared to the frequency of static behavior [18]. The process of discerning a tactile event with respect to a robot and the localization of such an event is prevalent independently

This work was supported by the Trinity College Summer Research Program. The authors would like to thank Kirkland Boyd from The University of Colorado Boulder for machining help, Andrew Pace from The University of Washington for technical guidance and Denisse Olemdo from Trinity College for feedback and support.

Divas Subedi, Elizabeth Schoemer, Digesh Chitrakar and Kevin Huang are with Trinity College, Dept. of Engineering, 300 Summit St., Hartford, CT 06106 USA {divas.subedi, elizabeth.schoemer, digesh.chitrakar, kevin.huang}@trincoll.edu

Yun-Hsuan Su is with Mount Holyoke College, Department of Computer Science, 50 College St., South Hadley, MA 01075 USA msu@mtholyoke.edu

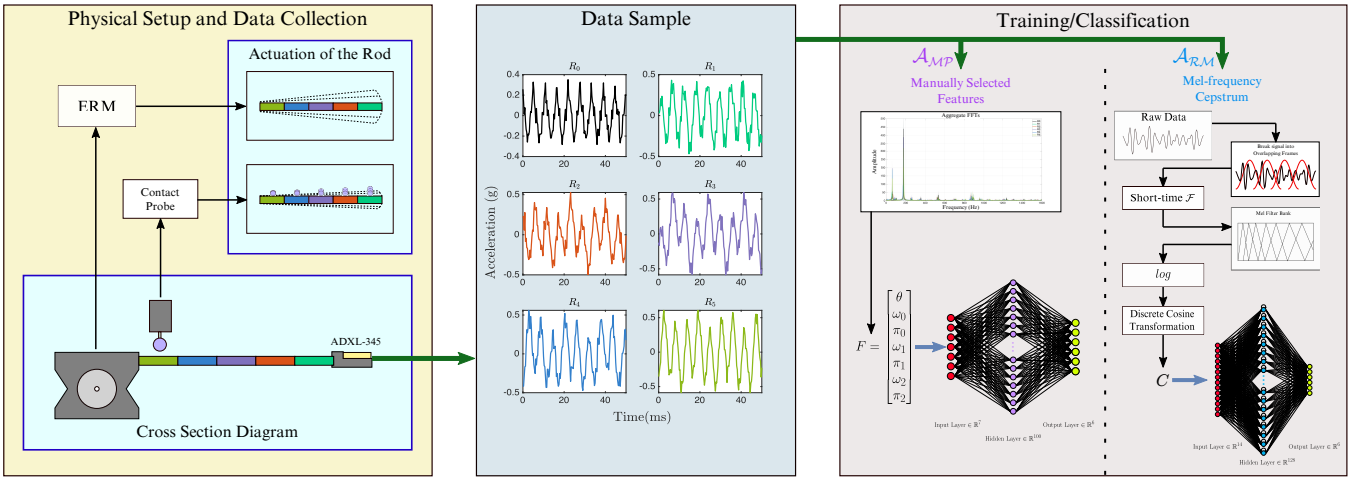

Fig. 2. Experimental workflow. The ERM actively actuates the rigid link, while contacts are made at appropriate locations between $R_1 - R_5$, R_0 is untouched. Inertial data is collected via the IMU. These data are then processed in two pathways, $\mathcal{A}_{\mathcal{MP}}$ and $\mathcal{A}_{\mathcal{RM}}$. The former uses manually selected features from transient behavior and spectral characteristics, and trains through a multi-class perceptron network. The latter uses Mels-frequency cepstral features, and generates a 98-length sequence of features per sample. These sequences are then used to train a bilateral long-short-term-memory network.

in previous rigid contact sensors. Monte Carlo approaches [19] and force propogation [20] can be used when sufficient external forces are present and the manipulator is equiped with torque sensors. Soft contact sensor arrays show promise in soft-robotics applications, yet suffer from hysteresis and nonlinearities [21]–[23].

2) Hardware Components: Recent accelerometer-based applications have explored environmental range-free position localization, as implemented through a H48C mounted on a Boe-Bot Robot Kit, and on-body device, or smartphone, positioning via microelectromechanical systems (MEMS) [24], [25]. Bulletti et al. [26] employed triaxial accelerometers for the detection of shallow landmines via the excitation of the soil-mine system with the production of a consistent sine wave by an acoustic source. While highly sensitive force-pressure sensors excel in terms of performance granularity, the cost of fabrication of piezoelectric arrays, including complex graphene-transfer configurations [27], diminishes the accessibility of such technology [28]. Accelerometers are an inexpensive and non-intrusive alternative method for varied data extraction, notably through a raw displacement lens and within the frequency domain for position and contact localization.

3) Signal Processing in Tactile Sensing: Göger et al [29] developed an anthropomorphic robot hand that utilized polyvinylidene fluoride (PVDF) sensors to classify contact patterns and slip detection for object manipulation and grasping. The short term Fourier transformation (STFT) generated input features for classification via principle component analysis (PCA). Similarly, Yi et al. [30] leveraged several classification algorithms such as support vectors (SVM) and k-nearest neighbors (kNN) to discriminate between various rough tactile sensors. Categorizing acceleration-based data for the classification of contact points often relies on the extraction of elements from the frequency spectrum and the subsequent correlation coefficients [25], [26]. Acceleration signals are also used to classify surface textures. Strese et al. [31] utilized such a method, coupled with various classifiers such as Gaussian Mixture Model (GMM) and Hidden-Markov-Models (HMM) to recognize texture.

4) Applications in Robotic Contact Localization: Tactile sensors, with an acute awareness of shifts in pressure and vibration, reproduce minute contextual details of a robotic environment for kinematic state observations [12]. In many commercial devices, the juxtaposition of binary tactile sensors with robotic joints provides information on external object intrusion with a robotic digit [32]. Locomotion in uncertain environmental conditions complicates the execution of maneuvers when rapid adaptations of motion are desired. Grimminger et al. [33] proposed an open-sourced foot sensor for a torque-controlled quadruped robot, gauging contact location in all directions for necessary adjustments. Human-robot interactions must avoid unexpected collisions for controller safety, necessitating a distinction between unintentional and intentional contact points, through observations of the frequency domain and response of Cartesian compliance controllers [34]. Similarly, the risk of fallout from machinery fault vibrations and assembly processes requires the discernment of mechanical fault location for appropriate replacement by analyzing vibrational responses [35], [36].

C. Contributions

This paper extends the granularity of contact localization using the authors' prior hardware model [37], an inexpensive rigid link model design that vibrates via an eccentric rotating mass motor (ERM). The method was inspired by a robust contact sensor manufactured by Backus et al. [18], [38] which discerned changes in the resonant frequency of a two link digit oscillated by a contact force. This study extends classification for increased contact points and an updated signal processing system. To the best of the authors' knowledge, this work is the first to simultaneously present:

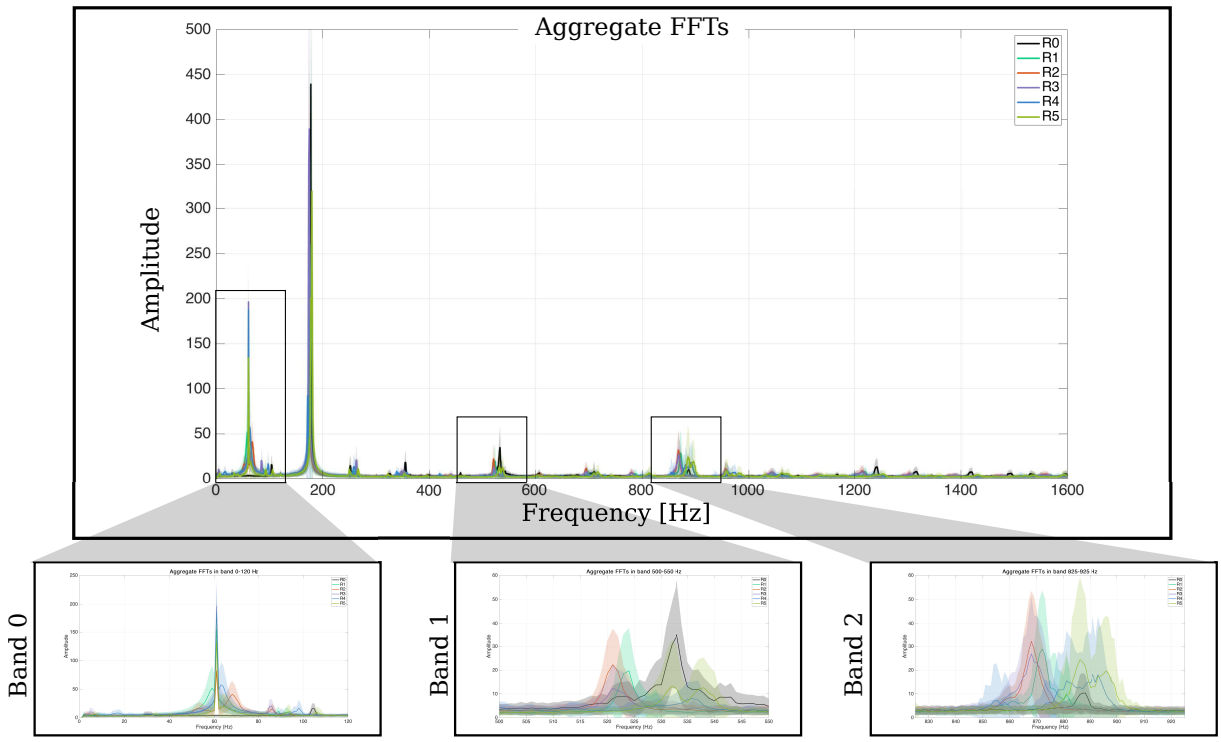

Fig. 3. Aggregate FFTs from all six contact classes $R_0 - R_5$. Three bands were empirically selected for feature extraction, and are shown as band 0 ([0,120]Hz), band 1 ([500,550]Hz), and band 2 ([825,925]Hz).

i) an inexpensive contact sensor constructed with off-the-shelf components that can be incorporated into robots with rigid links;
ii) contact localization on a rigid link based on active oscillation with an achieved granularity of distinction between non-contact and contact events approximately 2cm apart;
iii) a supervised deep learning network to distinguish various points of contact (among six classes: five contact locations and untouched) with accuracy over 98%.

II. Methods

The overall system workflow is depicted in Fig. 2. The procedural methodology for this research consisted of three components - system hardware (Section II-A); data collection (Section II-B); signal analysis (Section II-C) which also involves feature extraction and contact location classification.

A. System Hardware

A rigid link of 10.5cm length was implemented using ¼ inch UNC 20 threaded rod of ASTM A591 Zinc Coated Steel. This rigid link was affixed on a 3D printed PLA mount, which also housed the ERM. An ADXL 345 3-axis accelerometer was fixed to the terminal end of the rod, which was used to sample the mechanical response of the link with a sampling frequency of 3200Hz. The contact probe was manufactured by attaching a ⅝ inch rubber ball on a 3D printed arm and it was controlled by a standard precision MG995 metal gear servo. See [37] for more details.

TABLE I
Contact Locations - D is Distance to Terminal End

Contact Point	R_1	R_2	R_3	R_4	R_5
D[mm]	92.4	71.8	51.2	30.6	10.0

As shown in Table I, five points of contact were designated equally spaced out, with R_5 at the proximal end nearest the ERM, and R_1 near the terminal and accelerometer. The total length of the rod is approximately 105mm, including a 10mm buffer applied to both ends of the rigid link prior to the division of the five contact regions spaced 20.6mm apart.

B. Data Collection

The contact probe and the ERM actuator were automated using a Raspberry Pi to collect 150 time series samples drawn from each of the following six classes: (1) R_0, untouched, and contact at regions (2) R_1 (3) R_2 (4) R_3 (5) R_4 (6) R_5.

In each time series sample, the mechanical system is first at rest. The contact probe was then positioned via a servo mechanism corresponding to contact state (one $R_0 - R_5$ classes). The ERM was actuated for one second with no load and constant current. During this time, the accelerometer measured the 3-axis acceleration of the terminal end of the link at 3200 Hz. The contact probe was lifted while dynamics were allowed to attenuate for 180 seconds. For each class, this data collection process was repeated for 150 cycles, with an aggregate database of 900 one-second time series samples.

C. Feature Spaces

Two contact localization algorithms were proposed in this work - (1) $\mathcal{A}_{MP}$: Multiclass Perceptron - with manually selected features, F and (2) $\mathcal{A}_{RM}$: Recurrent Neural Network - with Mel-frequency cepstrum features C. The feature space constructions for F and C are described in the following subsections.

1) Manually Selected Features F : Manually selected features were determined by observations from data in both transient behavior and the frequency domain. i.e. the spectrum of the acceleration information in the vertical direction computed via the fast Fourier transformation (FFT).

Figure 3 depicts aggregate FFTs for all six classes with shaded confidence interval of one standard deviation. Mitra et. al. [37] demonstrated preliminary classification capability based on the peak-frequency and peak-prominence in the 0-100Hz band. Figure 3 shows that additional bands in the acceleration power spectra may hold discriminatory power between the classes. To that end, the following manually selected features were chosen:

$$F = \begin{bmatrix} \theta & \omega_0 & \pi_0 & \omega_1 & \pi_1 & \omega_2 & \pi_2 \end{bmatrix}^T \tag{1}$$

where θ is the inverse tangent of ratio of RMS vertical and horizontal acceleration respectively, ω_i denotes peak frequency within band i, and π_i is peak prominence in band i. Bands 0, 1 and 2 include [0, 120] Hz, [500-550] Hz, and [825-925] Hz respectively (these were empirically determined from Fig. 3). Prominence of peak is defined as the peak value minus either the left or right trough value, whichever is greater.

Prior to classification, the feature space was pre-processed and normalized along all feature dimensions via Z-score normalization. Figure 4 shows the distribution of each feature stratified by contact region.

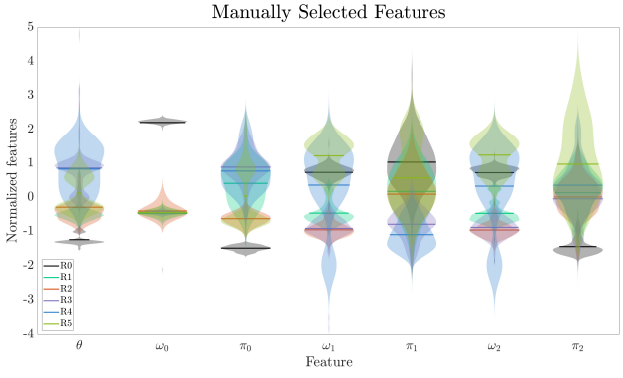

Fig. 4. F Feature Space - bean plots show distributions of feature values for each contact location class. These manually selected features originate from both transient behavior and FFT based parameters as described by (1). Tick marks in the bean plots represent the means of the feature distributions.

2) Mel-Frequency Cepstrum Features, C: The mel-frequency cepstral coefficient (MFCC) were primarily developed for audio signal recognition. Recently, this feature extraction method has been used for various purposes including hand gesture [39], and surface texture recognition [31]. For the purpose of this experiment, MFCC was deployed to extract 14 coefficients (as per default in MATLAB Audio Toolbox™) from each time series sample. The implemented algorithm segmented the time signal into overlapping frames, with 30ms frame width and 10ms overlap - the maximum window size using STFT for MFCC. The MFCC extraction was calculated as in [40]. Specifically, the signal within the frame was examined in the frequency domain using STFT

$$X(k) = \sum_{n=0}^{N-1} x(n) e^{\frac{-jnk}{N} 2\pi}; \quad 0 \leq k \leq N-1 \tag{2}$$

The Fourier transformed signal was mapped from physical frequency to mel frequency as

$$f_{mel} = 2595 \log_{10}\left(1 + \frac{f}{700}\right) \tag{3}$$

followed by a series of band-pass filters (mel-filter bank). The Mel spectrum was then obtained by multiplying the power spectrum by each of the mel weighting filters

$$s(m) = \sum_{k=0}^{N-1} \left[|X(k)|^2 H_m(k) \right]; \quad 0 < m < M-1 \tag{4}$$

, where H_m is the m^{th} weighting filter and M is the total number of filters used. In this experiment, the Audio Toolbox™ default of 40 triangular filters were used. Finally, the coefficients were calculated by applying the Discrete Cosine Transformation, as in

$$C(n) = \sum_{m=0}^{M-1} \log_{10}(s(m)) \cos\left(\frac{\pi n (m - 0.5)}{M}\right) \tag{5}$$

The first 14 coefficients constitute the $\mathcal{A}_{RM}$ feature space, i.e. $0 \leq n \leq 13$ in (5).

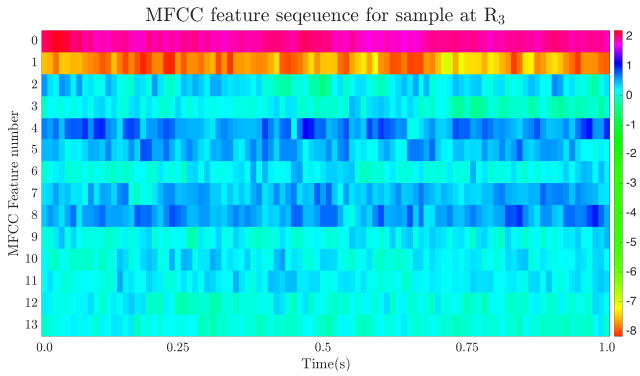

Fig. 5. A sample sequence of 98 MFCC coefficients generated over the one second acceleration time series sample for a contact at R_3. These features arranged in a sequence are amenable to classification by recurrent networks.

With window size of 30ms and 10ms of overlap, each one second time series sample generates 98 sequential sets of the 14 features in C. Figure 5 shows an example of extracted MFCC features from a single time series.

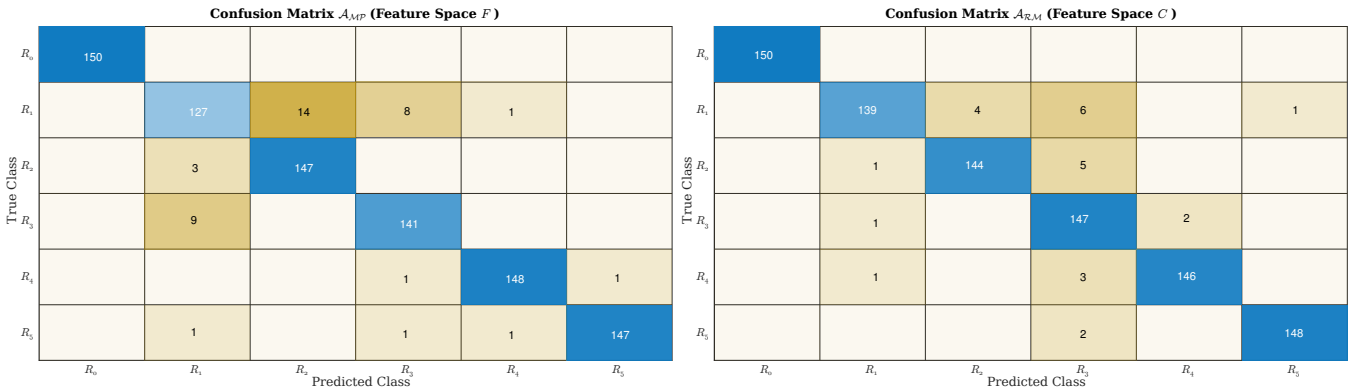

Fig. 6. Confusion matrices depicting contact location classification results from the 5-fold evaluation using $\mathcal{A}_{MP}$ (left) and $\mathcal{A}_{RM}$ (right) respectively.

Prior to classification, the data were pre-processed and normalized along all feature dimensions via Z-score normalization. Figure 7 depicts the distribution of each feature stratified by contact region.

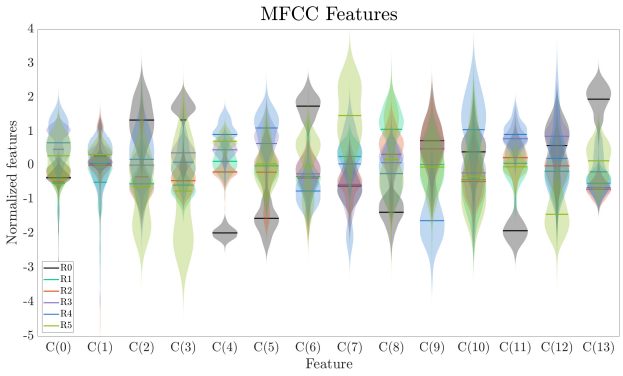

Fig. 7. C Feature Space - bean plots show distributions of feature values for each contact location class. The 14 features are the first 14 MFCC coefficients as calculated with (2-5). Tick marks in the bean plots represent the means of the feature distributions.

D. Classifiers

Both F and C data-sets were uniformly segmented within the six classes into a split of 80% training and 20% testing data. The training sets were then used to train two different types of supervised agents, $\mathcal{A}_{MP}$: Multi-class Perceptron for F and $\mathcal{A}_{RM}$: Recurrent Neural Network for C. Perceptron networks are well suited for single feature-vector classification. On the other hand, the Mels-frequency cepstral features generated sequences of feature vectors, which are amenable to recurrent neural networks.

In $\mathcal{A}_{MP}$, the seven features in F served as inputs to a single layer of 100 perceptrons using scaled conjugate gradient backpropogation to optimize cross entropy. This network was used to learn the six contact class outputs, $R_0 - R_5$. For $\mathcal{A}_{RM}$, the sequences of 98 C feature vectors per sample were used to train a bidirectional long short term memory recurrent neural network with 128 hidden units, sigmoid gate activation and hyperbolic tangent state activation.

III. Results and Discussion

The classification performances respectively using $\mathcal{A}_{MP}$ and $\mathcal{A}_{RM}$ were analyzed with 5-fold cross validation using 180 test data samples (20% of the dataset) per fold. The overall results are presented as two confusion matrices in Fig 6. The precision, recall, accuracy and F1-score at each contact point (R0 - R5) were evaluated for both classifiers as tabulated in Tables II and III.

TABLE II
Multi-class Perceptron Classifier ($\mathcal{A}_{MP}$) Performance

Class	Precision	Recall	Accuracy	F1-score
R_0	1.0	1.0	1.0	1.0
R_1	0.9071	0.8467	0.9600	0.8759
R_2	0.9130	0.9800	0.9811	0.9453
R_3	0.9338	0.9400	0.9789	0.9369
R_4	0.9867	0.9867	0.9956	0.9867
R_5	0.9932	0.9800	0.9956	0.9866

The classification performances with no contact (R_0) are highlighted light orange in tables and the best performed class under each evaluation metric is highlighted in green. In summary, an overall accuracy of 95.56% is achieved using $\mathcal{A}_{MP}$ and 97.11% using $\mathcal{A}_{RM}$.

TABLE III
Bi-LTSM Classifier ($\mathcal{A}_{RM}$) Performance

Class	Precision	Recall	Accuracy	F1-score
R_0	1.0	1.0	1.0	1.0
R_1	0.9789	0.9267	0.9844	0.9521
R_2	0.9730	0.9600	0.9889	0.9664
R_3	0.9018	0.9800	0.9789	0.9393
R_4	0.9865	0.9733	0.9933	0.9799
R_5	0.9933	0.9867	0.9967	0.9900

A. Analysis of Results

Several observations can be drawn from these results. From the confusion matrices, results suggest that:

- touched classes, that is $R_1 - R_5$, are readily distinguished from untouched R_0;
- in general, contacts furthest from the ERM were more difficult to classify;
- both $\mathcal{A}_{\mathcal{MP}}$ and $\mathcal{A}_{\mathcal{RM}}$ misclassifications tend to predict contact more proximal than true contact location;
- distinguishing contact in region class R_1 is particularly challenging for $\mathcal{A}_{\mathcal{MP}}$, resulting in a total of 23 false negatives and 13 false positives;
- both $\mathcal{A}_{\mathcal{MP}}$ and $\mathcal{A}_{\mathcal{RM}}$ exhibited the most false positives classifying region R_1 contact. $\mathcal{A}_{\mathcal{MP}}$ also showed the most false negatives for R_1, while $\mathcal{A}_{\mathcal{RM}}$'s most false negatives were from the R_3 class;

From Tables II and III, results show that:

- $\mathcal{A}_{\mathcal{RM}}$ classified contacts at point R_5 consistently better than other classes, whereas $\mathcal{A}_{\mathcal{MP}}$ classified contacts at R_4, R_5 better than other classes;
- $\mathcal{A}_{\mathcal{RM}}$ did not exhibit any metric below 0.9 for any class, while $\mathcal{A}_{\mathcal{MP}}$ had two;
- precision for R_5 is the greatest amongst touched classes for both methods, suggesting that R_5 is the most robust in-contact class to classify.

B. Future Directions

This work presents a low-cost, non-intrusive method of detecting contact locations at a higher granularity than the authors' prior work. With that said, there is room for further improvement to increase applicability. Future work may include:

- Actuation modality: the current prototype uses a general purpose ERM, which is unable to modulate its amplitude and frequency independently. For the purpose of this experiment, 1.5V is applied to the ERM with no changing load, which oscillates the rigid link at 170 Hz, without modulation specificity;
- For the hand-picked features, peak frequency and its prominence at three different bands are utilized. More experiments can be conducted at various bands to evaluate the performance. Similarly, the parameters of MFCC features can be changed and tested to improve performance;
- Expansion of the data-set is also a viable option to extend the capabilities of the sensor. Only acceleration in the z-axis is utilized. By leveraging more dimensions of acceleration, feature spaces can possibly be more unique and discriminatory, helping classify more regions;
- The orientation and inherent physical features of the rigid link may be adjusted for a more in-depth preview of contact methodologies in dynamic structures. A robot end effector may frequently be in motion, so robot state parameters may be incorporated for more training;
- As it stands, the rod is symmetrical radially along the axial direction, so while region of contact can be distinguished, it is not precise enough to determine radially contact position. A radially asymmetric rod might be used to obtain directionality of contact.

IV. Conclusion

The baseline approach in the authors' prior work [37] considered a reduced feature space of $[\omega_0, \pi_0]$ from F and with a classification accuracy of 90%. The previous approach considered the unsupervised method of Gaussian Mixture Models and a simple supervised logistic regression. With more contact locations and features, the proposed method is promising, as it presents more complexity and discrimination at higher granularity of localization.

This study presents a novel low-cost system and two contact localization approaches - $\mathcal{A}_{MP}$ and $\mathcal{A}_{RM}$ that are able to distinguish six distinct contact states (five contact locations and untouched) which can be incorporated in rigid links with minimal effort. $\mathcal{A}_{MP}$ utilized manually selected features from transient behavior and spectral characteristics to train a multi-class perceptron network. $\mathcal{A}_{RM}$ used sequences of Mel-frequency cepstral features as a feature space and a bi-directional LSTM. An approximate spacing of two centimeters between contact locations was used in this work. Both proposed approaches achieve an outstanding classification accuracy of more than 95%, and a 100% accuracy for detecting events of contact (R_0 versus R_{1-5}).

References

[1] U. Naik, S. Bhuatara, and B. Chougala, "An experimental framework for automated bed localization and drug identification using zigbee signal strength and mobile robot," in *2019 IEEE International Conference on Distributed Computing, VLSI, Electrical Circuits and Robotics (DISCOVER)*, 2019, pp. 1–6.

[2] K. J. Vänni and S. E. Salin, "A need for service robots among health care professionals in hospitals and housing services," in *International Conference on Social Robotics*. Springer, 2017, pp. 178–187.

[3] K. Huang, D. Chitrakar, F. Rydén, and H. J. Chizeck, "Evaluation of haptic guidance virtual fixtures and 3d visualization methods in telemanipulation—a user study," *Intelligent Service Robotics*, vol. 12, no. 4, pp. 289–301, 2019.

[4] O. Kroemer, S. Niekum, and G. Konidaris, "A review of robot learning for manipulation: Challenges, representations, and algorithms." *J. Mach. Learn. Res.*, vol. 22, pp. 30–1, 2021.

[5] K. Huang, D. Chitrakar, R. Mitra, D. Subedi, and Y.-H. Su, "Characterizing limits of vision-based force feedback in simulated surgical tool-tissue interaction," in *2020 42nd Annual International Conference of the IEEE Engineering in Medicine & Biology Society (EMBC)*. IEEE, 2020, pp. 4903–4908.

[6] B. Hannaford, J. Rosen, D. W. Friedman, H. King, P. Roan, L. Cheng, D. Glozman, J. Ma, S. N. Kosari, and L. White, "Raven-ii: an open platform for surgical robotics research," *IEEE Transactions on Biomedical Engineering*, vol. 60, no. 4, pp. 954–959, 2012.

[7] Y.-H. Su, Y. Sosnovskaya, B. Hannaford, and K. Huang, "Securing robot-assisted minimally invasive surgery through perception complementarities," in *2020 Fourth IEEE International Conference on Robotic Computing (IRC)*. IEEE, 2020, pp. 41–47.

[8] S. Haddadin, A. Albu-Schaffer, A. De Luca, and G. Hirzinger, "Collision detection and reaction: A contribution to safe physical human-robot interaction," in *2008 IEEE/RSJ International Conference on Intelligent Robots and Systems*. IEEE, 2008, pp. 3356–3363.

[9] D. F. Gomes, Z. Lin, and S. Luo, "Blocks world of touch: Exploiting the advantages of all-around finger sensing in robot grasping," *Frontiers in Robotics and AI*, vol. 7, 2020.

[10] P. S. Girão, P. M. P. Ramos, O. Postolache, and J. M. D. Pereira, "Tactile sensors for robotic applications," *Measurement*, vol. 46, no. 3, pp. 1257–1271, 2013.

[11] R. S. Dahiya and M. Valle, *Robotic tactile sensing: technologies and system*. Springer Science & Business Media, 2012.

[12] M. Hafez, "Tactile interfaces: technologies, applications and challenges," *The Visual Computer*, vol. 23, no. 4, pp. 267–272, 2007.

[13] D. Kim and Y.-L. Park, "Contact localization and force estimation of soft tactile sensors using artificial intelligence," in *2018 IEEE/RSJ International Conference on Intelligent Robots and Systems (IROS)*. IEEE, 2018, pp. 7480–7485.

[14] U. Kim, D.-H. Lee, Y. B. Kim, D.-Y. Seok, and H. R. Choi, "A novel six-axis force/torque sensor for robotic applications," *IEEE/ASME Transactions on Mechatronics*, vol. 22, no. 3, pp. 1381–1391, 2016.

[15] M. Farag, A. N. A. Ghafar, and M. H. ALSIBAI, "Real-time robotic grasping and localization using deep learning-based object detection technique," in *2019 IEEE International Conference on Automatic Control and Intelligent Systems (I2CACIS)*, 2019, pp. 139–144.

[16] A. Molchanov, O. Kroemer, Z. Su, and G. S. Sukhatme, "Contact localization on grasped objects using tactile sensing," in *2016 IEEE/RSJ International Conference on Intelligent Robots and Systems (IROS)*. IEEE, 2016, pp. 216–222.

[17] W. McMahan, J. M. Romano, and K. J. Kuchenbecker, "Using accelerometers to localize tactile contact events on a robot arm," in *Proceedings of Workshop on Advances in Tactile Sensing and Touch-Based Human-Robot Interaction, ACM/IEEE International Conference on Human-Robot Interaction*. Citeseer, 2012.

[18] S. B. Backus and A. M. Dollar, "Robust, inexpensive resonant frequency based contact detection for robotic manipulators," in *2012 IEEE International Conference on Robotics and Automation*. IEEE, 2012, pp. 1514–1519.

[19] A. Zwiener, R. Hanten, C. Schulz, and A. Zell, "Armcl: Arm contact point localization via monte carlo localization," in *2019 IEEE/RSJ International Conference on Intelligent Robots and Systems (IROS)*. IEEE, 2019, pp. 7105–7111.

[20] D. Popov and A. Klimchik, "Real-time external contact force estimation and localization for collaborative robot," in *2019 IEEE International Conference on Mechatronics (ICM)*, vol. 1. IEEE, 2019, pp. 646–651.

[21] D. Kim and Y.-L. Park, "Contact localization and force estimation of soft tactile sensors using artificial intelligence," in *2018 IEEE/RSJ International Conference on Intelligent Robots and Systems (IROS)*. IEEE, 2018, pp. 7480–7485.

[22] L. Costi, T. G. Thuruthel, and F. Iida, "Topological study on the design of soft strain sensors for simultaneous multi-point contact localization," in *2021 IEEE 4th International Conference on Soft Robotics (RoboSoft)*. IEEE, 2021, pp. 555–558.

[23] Y. Wang, H. Wang, Z. Liu, and W. Chen, "Visual servo-collision avoidance hybrid task by considering detection and localization of contact for a soft manipulator," *IEEE/ASME Transactions on Mechatronics*, vol. 25, no. 3, pp. 1310–1321, 2020.

[24] C.-H. Hsu and C.-H. Yu, "An accelerometer based approach for indoor localization," in *2009 Symposia and Workshops on Ubiquitous, Autonomic and Trusted Computing*. IEEE, 2009, pp. 223–227.

[25] K. Fujinami, "On-body smartphone localization with an accelerometer," *Information*, vol. 7, no. 2, p. 21, 2016.

[26] A. Bulletti, S. Valentini, F. Cioria, G. Borgioli, M. Calzolai, L. Capineri, and L. Masotti, "Silicon micromachined accelerometers for the detection of compliant anti-personnel landmines," in *SENSORS, 2008 IEEE*. IEEE, 2008, pp. 1159–1162.

[27] N. Yogeswaran, W. Navaraj, S. Gupta, F. Liu, V. Vinciguerra, L. Lorenzelli, and R. Dahiya, "Piezoelectric graphene field effect transistor pressure sensors for tactile sensing," *Applied Physics Letters*, vol. 113, no. 1, p. 014102, 2018.

[28] R. Ramalingame, A. Lakshmanan, F. Müller, U. Thomas, and O. Kanoun, "Highly sensitive capacitive pressure sensors for robotic applications based on carbon nanotubes and pdms polymer nanocomposite," *Journal of Sensors and Sensor Systems*, vol. 8, no. 1, pp. 87–94, 2019.

[29] D. Goger, N. Gorges, and H. Worn, "Tactile sensing for an anthropomorphic robotic hand: Hardware and signal processing," in *2009 IEEE International Conference on Robotics and Automation*, 2009, pp. 895–901.

[30] Z. Yi, Y. Zhang, and J. Peters, "Bioinspired tactile sensor for surface roughness discrimination," *Sensors and Actuators A: Physical*, vol. 255, pp. 46–53, 2017. [Online]. Available: https://www.sciencedirect.com/science/article/pii/S0924424716311992

[31] M. Strese, J.-Y. Lee, C. Schuwerk, Q. Han, H.-G. Kim, and E. Steinbach, "A haptic texture database for tool-mediated texture recognition and classification," in *2014 IEEE International Symposium on Haptic, Audio and Visual Environments and Games (HAVE) Proceedings*, 2014, pp. 118–123.

[32] H. Hu and J. Q. Gan, "Sensors and data fusion algorithms in mobile robotics," *Technical Report: CSM-422, Department of Computer Science*, 2005.

[33] F. Grimminger, A. Meduri, M. Khadiv, J. Viereck, M. Wüthrich, M. Naveau, V. Berenz, S. Heim, F. Widmaier, T. Flayols, *et al.*, "An open torque-controlled modular robot architecture for legged locomotion research," *IEEE Robotics and Automation Letters*, vol. 5, no. 2, pp. 3650–3657, 2020.

[34] A. Kouris, F. Dimeas, and N. Aspragathos, "A frequency domain approach for contact type distinction in human–robot collaboration," *IEEE robotics and automation letters*, vol. 3, no. 2, pp. 720–727, 2018.

[35] C. Bergqvist, B. A. Soderquist, and A. Wernersson, "On combining accelerometers, force/torque sensors, and electrical sensing for detecting contact errors during assembly," in *Proceedings of IEEE/RSJ International Conference on Intelligent Robots and Systems (IROS'94)*, vol. 3. IEEE, 1994, pp. 1736–1743.

[36] B. Li, M.-Y. Chow, Y. Tipsuwan, and J. C. Hung, "Neural-network-based motor rolling bearing fault diagnosis," *IEEE transactions on industrial electronics*, vol. 47, no. 5, pp. 1060–1069, 2000.

[37] R. Mitra, K. Boyd, D. Subedi, D. Chitrakar, E. Aldrich, A. Swamy, and K. Huang, "Contact sensing via active oscillatory actuation," in *2020 3rd International Conference on Mechatronics, Robotics and Automation (ICMRA)*. IEEE, 2020, pp. 99–104.

[38] S. B. Backus and A. M. Dollar, "Robust resonant frequency-based contact detection with applications in robotic reaching and grasping," *IEEE/ASME Transactions on Mechatronics*, vol. 19, no. 5, pp. 1552–1561, 2014.

[39] S. Gupta, J. Jaafar, W. F. wan Ahmad, and A. Bansal, "Feature Extraction Using Mfcc," *Signal & Image Processing : An International Journal*, vol. 4, no. 4, pp. 101–108, Aug. 2013. [Online]. Available: http://www.aircconline.com/sipij/V4N4/4413sipij08.pdf

[40] K. S. Rao and A. K. Vuppala, *Speech processing in mobile environments*. Springer, 2014.